



OPEN

## Application of the principle of collapsed distributions to the detection of faulty elements in square grid antenna arrays

David Michael Parkinson-Oreiro<sup>1</sup>, María Elena López-Martín<sup>2</sup>,  
Juan Antonio Rodríguez-González<sup>1</sup> & Francisco José Ares-Pena<sup>1</sup>✉

The following paper presents an application of the principle of collapsed distributions to the diagnosis of square grid planar antenna arrays. The principle states that each azimuthal cut of a planar array pattern (array factor), with  $\phi = \phi_o$ , is equivalent to the pattern generated by a linear array. The linear array is obtained by projecting all of the excitations of the planar antenna on to the line  $\phi = \phi_o$ . This idea is used to develop an algorithm for detecting faulty elements in damaged planar arrays, where only on-off faults are considered. The algorithm uses far-field complex samples of the damaged pattern taken along the  $\phi = 0^\circ, 45^\circ, 90^\circ$  cuts. It uses this information to perform an exhaustive search to find the three collapsed linear arrays (in the specified directions) that best match the samples of the damaged pattern. Thus, the coordinates of the faulty elements along the three mentioned axes can be easily obtained. The algorithm was applied here to the diagnosis of a 76-element square grid antenna with circular boundary and quadrantal symmetry.

Antenna arrays are used in a wide range of applications, including satellite communications, remote sensing, and radar systems. In particular, the square grid planar array is extensively used, because its orderly lattice structure allows for a simpler design of the power distribution network<sup>1</sup>. This set-up is preferred even when physical mounting or radiation pattern requirements dictate a circular or elliptical aperture. In such cases, the specific aperture is attained by “lopping off” elements in a square grid array, as can be seen in Fig. 1.

Arrays typically consist of a large number of radiating elements, and the possibility of failure of some of these is very high. Such element failures cause sharp variations in the field intensity, leading to an increase of the side-lobes in the power pattern<sup>2</sup>. Thus, an effective and reliable diagnostic tool for large antenna arrangements is essential<sup>3,4</sup>. Diagnosis is usually conducted by analysing samples of the damaged radiation pattern, and it is very important that the number of samples required by the method is as small as possible relative to the number of radiating elements in the array<sup>5-7</sup>.

The Moore-Penrose matrix pseudoinversion has proven to be an effective diagnostic tool<sup>8</sup> but generally requires a large number of samples. The use of case-based reasoning has also been studied. This system identifies the elements that are most likely to be defective, significantly reducing the computational costs of detection<sup>9</sup>. However, this does not provide a final solution, but rather a starting point for the use of other methods such as genetic algorithms<sup>3,4</sup>.

In the recent literature, many variants of compressive sensing (CS) methods have been used because they are able to recover sparse signals from under-sampled measurements. This is ideal, since faulty elements typically constitute a small fraction of the total array and are hence sparse. Most of these techniques require the acquisition of both amplitude and phase far-field measurements of the damaged pattern<sup>5,6</sup>. Morabito et al. leverage the CS framework, casting the diagnosis as a convex programming (CP) problem to enable rapid diagnosis from phaseless far-field data<sup>10,11</sup>. They further adapt this methodology to near-field measurements and facilitate the detection of phase faults<sup>7</sup>. The latter development has recently been extended to the case of phaseless far-field samples<sup>12</sup>.

In this article we propose a method based on the collapsed distribution principle<sup>13-15</sup>, which provides reliable diagnosis of square grid planar arrays by using far-field measurements along three azimuthal cuts of the

<sup>1</sup>Radiating Systems Group, Department of Applied Physics, University of Santiago de Compostela, 15782 Santiago de Compostela, Spain. <sup>2</sup>Department of Morphological Sciences, University of Santiago de Compostela, 15782 Santiago de Compostela, Spain. ✉email: francisco.ares@usc.es

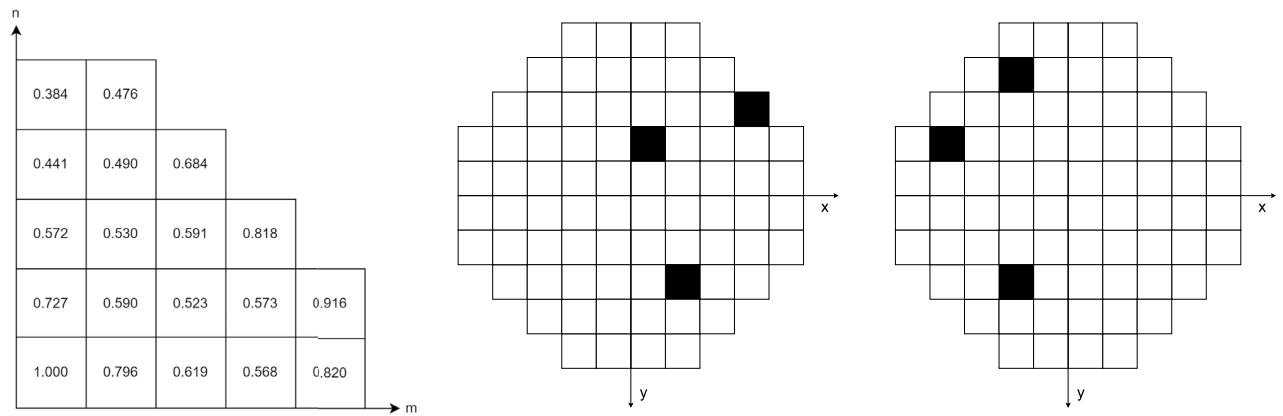


**Fig. 1.** One quadrant of the 76-element square grid antenna with excitations (left); the two first examples of 3-fault configurations used in the present study (center and right). X, Y coordinates are measured from 1 to 10 increasing from left to right and from top to bottom, respectively.

damaged pattern. The number of samples required for the method to be successful depends on the size of the measurement error, and both the amplitude and phase must be known to solve indeterminacy problems related to the symmetry properties of the arrays. This is the case of the antenna used in this study, which has quadrantal symmetry. The case of asymmetrical arrays is favourable because it doesn't require knowledge of the phase.

The main advantage of this method is the fact that it only requires the measurement of three  $\phi$ -cuts of the radiation pattern: the  $\phi = 0^\circ$  (or X-axis) cut, the  $\phi = 90^\circ$  (or Y-axis) cut, and the  $\phi = 45^\circ$  cut. Meanwhile, most of the fault detection methods, like compressive sensing, need to sample the whole radiation pattern.

## Results

The algorithm devised in the methods section was tested on a 76-element square grid antenna with circular boundary and quadrantal symmetry, shown in Fig. 1. The specific synthesis of the antenna was taken from the dissertation by Kim, Y.U.<sup>13</sup>: side-lobes at  $-20, -21, -22, -23$  dB along the  $\phi = 0^\circ$  cut relative to the height of the main beam, and  $-30, -31, -32, -33$  dB side-lobe levels along the  $\phi = 90^\circ$  cut. Anywhere in between these planes, side-lobe levels vary smoothly using an envelope function. The corresponding excitations, which are real and positive, are also shown in Fig. 1 (left) as one quadrant of the whole antenna.

Ten different error configurations of three faulty elements were randomly generated, and only absolute failure of the elements (on-off faults) was considered. The tests were run for five different numbers of samples of the damaged pattern: 30, 45, 90, 180 and 360 samples. Measurement errors of the damaged pattern were also simulated, both in amplitude and phase, by artificially introducing a uniform random distribution in each sample, centered at the true value and with maximum errors of  $\Delta_{\text{dB}} = \pm 0.5\text{dB}, \pm 1\text{dB}$  and  $\Delta_{\text{ph}} = \pm 2.5^\circ, \pm 5^\circ$ . The parameters were tuned so that the algorithm only searched for failed configurations of up to four faulty elements, and it only considered percentages of failure of the elements of the collapsed linear arrays between 50% and 100% of the original value. Anything smaller than 50% would waste computing time, as the number of faulty elements in the antenna is not sufficient to cause such a large defect in the collapsed arrays. The algorithm was run ten times for each configuration in order to obtain a meaningful statistic. The results of the study considering the measurement error are presented in Tables 1 and 2, while the case for zero measurement error is shown in Table 3. For the latter, the algorithm was run only once for each configuration, since there is no randomness in the results. Some examples of the fault configurations used in the study are also shown in Fig. 1.

The need for complex samples of the far-field pattern is due to the fact that the antenna used in the tests has quadrantal symmetry. When working with only the amplitude of the pattern, the algorithm can detect the distance from the X and Y axes of the faulty elements, but it is not able to discern which side the fault is on. The phase of the pattern provides the information required to solve this problem. Nevertheless, if the antenna is asymmetric with respect to the X and Y axes, the amplitude alone is sufficient to correctly recover the positions of the faulty elements.

## Discussion

The study findings show that increasing the number of samples of the damaged pattern improves the success of the fault detection algorithm. Moreover, when the size of the measurement errors allowed is reduced, the number of samples required to yield a high rate of success is also greatly decreased. In most of the runs in which the algorithm failed to detect the correct faulty element configuration, the algorithm correctly predicted the positions of the three targeted faults, but incorrectly predicted a fourth fault.

Application of the algorithm to the diagnosis of larger antennas, would require knowledge of the partial single-fault patterns,  $F_n^p(\theta)$ , mentioned in the methods section, with a finer mesh of the index  $p$ . This is because for large arrays, faulty elements will cause smaller defects in the excitations of the collapsed linear arrays. Thus, in most cases, failure of the collapsed excitations will only range between 90% and 100% of the original value.

3 defective elements, $\Delta_{dB} = \pm 0.5dB$ , $\Delta_{ph} = \pm 2.5^\circ$				
30 samples (M/N = 0.39)		45 samples (M/N = 0.59)		Failing element positions
t(s)	Success	t(s)	success	
9	7/10	9	10/10	(7, 8), (9, 3), (6, 4)
9	10/10	9	10/10	(4, 8), (2, 4), (4, 2)
9	10/10	9	10/10	(5, 9), (9, 6), (6, 3)
9	5/10	9	9/10	(6, 4), (9, 4), (5, 1)
9	8/10	9	10/10	(4, 1), (7, 4), (9, 4)
9	10/10	9	10/10	(9, 5), (9, 7), (4, 9)
9	7/10	9	10/10	(6, 10), (5, 9), (8, 8)
9	7/10	9	10/10	(5, 7), (10, 5), (6, 6)
9	9/10	9	10/10	(2, 5), (1, 5), (6, 8)
9	8/10	9	10/10	(10, 6), (6, 1), (5, 1)
<b>9</b>	<b>81/100</b>	<b>9</b>	<b>99/100</b>	<b>Average</b>

**Table 1.** Success rate and run time of the algorithm with a maximum measurement error of  $\pm 0.5dB$  and  $\pm 2.5^\circ$ . M/N is the ratio of the number of samples M to the number of elements N in the array.

3 defective elements, $\Delta_{dB} = \pm 1dB$ , $\Delta_{ph} = \pm 5^\circ$						
90 samples (M/N = 1.18)		180 samples (M/N = 2.36)		360 samples (M/N = 4.73)		Failing element positions
t(s)	Success	t(s)	Success	t(s)	Success	
8	8/10	10	8/10	14	10/10	(7, 8), (9, 3), (6, 4)
8	9/10	10	10/10	17	10/10	(4, 8), (2, 4), (4, 2)
10	10/10	12	10/10	17	10/10	(5, 9), (9, 6), (6, 3)
11	8/10	13	8/10	17	9/10	(6, 4), (9, 4), (5, 1)
11	8/10	12	9/10	17	9/10	(4, 1), (7, 4), (9, 4)
10	8/10	12	10/10	17	10/10	(9, 5), (9, 7), (4, 9)
10	7/10	12	10/10	17	10/10	(6, 10), (5, 9), (8, 8)
10	9/10	12	9/10	17	10/10	(5, 7), (10, 5), (6, 6)
10	8/10	12	10/10	17	10/10	(2, 5), (1, 5), (6, 8)
11	8/10	12	9/10	17	10/10	(10, 6), (6, 1), (5, 1)
<b>9.9</b>	<b>83/100</b>	<b>11.7</b>	<b>93/100</b>	<b>16.7</b>	<b>98/100</b>	<b>Average</b>

**Table 2.** Success rate and run time of the algorithm with a maximum measurement error of  $\pm 1dB$  and  $\pm 5^\circ$ . M/N is the ratio of the number of samples M to the number of elements N in the array.

3 defective elements, No measurement error		
Time (s)	# of samples required for success	Failing element positions
9	18	(7, 8), (9, 3), (6, 4)
9	18	(4, 8), (2, 4), (4, 2)
9	27	(5, 9), (9, 6), (6, 3)
9	27	(6, 4), (9, 4), (5, 1)
9	24	(4, 1), (7, 4), (9, 4)
9	15	(9, 5), (9, 7), (4, 9)
9	24	(6, 10), (5, 9), (8, 8)
9	27	(5, 7), (10, 5), (6, 6)
9	15	(2, 5), (1, 5), (6, 8)
9	18	(10, 6), (6, 1), (5, 1)
<b>9</b>	<b>21</b>	<b>Average</b>

**Table 3.** Minimum number of samples required for the algorithm to succeed when measurement errors are not considered.

Therefore, there would be no sense in exploring values of the index  $p$  smaller than 9. Instead, the interval from 90% to 100% should be used, possibly in steps of 1% or 2%.

## Methods

If mutual coupling between elements of the antenna is neglected, the total field pattern of the array can be expressed as the vector sum of the fields radiated by the individual elements. Moreover, if the elements are identical and equally oriented, the total field pattern can be expressed as the product of two quantities: the element factor and the array factor. The element factor corresponds to the field of one element and is a vector quantity. On the other hand, the array factor is a scalar quantity, independent of the element characteristics and is calculated as the sum of directionally weighted phasors. This factor contains information about the geometrical configuration of the elements and the distribution of the complex excitations, and it has a major influence on antenna performance. For commonly used elements, such as dipoles and slots, the element factor is a broad pattern. Hence, the element factor can often be ignored. In this case, the antenna corresponds to an array of hypothetical isotropic radiators<sup>13,14</sup>.

## The principle of collapsed distributions

The array factor of a planar array of  $M \times N$  elements laying in the  $xy$  plane arranged in a square lattice with spacing  $d$  is given by<sup>14</sup>

$$F(\theta, \phi) = \sum_{m=1}^M \sum_{n=1}^N I_{mn} \exp \{ jkd \sin \theta (m \cos \phi + n \sin \phi) \} \quad (1)$$

where  $I_{mn}$  is the relative excitation of the  $m$ th element. Considering a specific  $\phi$ -cut with  $\phi = \phi_o$  parametrized by two integers  $p, q \in \mathbb{Z}$  as

$$\tan \phi_o = \frac{\sin \phi_o}{\cos \phi_o} = \frac{q}{p} \quad (2)$$

Then, using the fundamental trigonometric identity

$$\begin{cases} \sin \phi_o = Aq \\ \cos \phi_o = Ap \end{cases} \text{ with } A \in \mathbb{R} \implies A = \frac{1}{\sqrt{q^2 + p^2}} \quad (3)$$

and substituting this parametrization in Eq. 1, the following expression is obtained for the array factor evaluated at a specific  $\phi$ -cut<sup>13–15</sup>:

$$F(\theta, \phi_o) = \sum_{m=1}^M \sum_{n=1}^N I_{mn} \exp \left\{ j \frac{kd \sin \theta (mp + nq)}{\sqrt{p^2 + q^2}} \right\} \quad (4)$$

Both summations can be combined into a single expression running over the index  $l = mp + nq$ , which ranges from  $(p + q)$  to  $(Mp + Nq)$ . For each value of  $l$ , there will be several excitations  $I_{mn}$  satisfying  $l = mp + nq$ , so these can be grouped as follows.

$$X_l = \sum_{m=1}^M \sum_{n=1}^N \varepsilon_{mn} I_{mn} \quad \text{with} \quad \varepsilon_{mn} = \begin{cases} 1 & \text{if } mp + nq = l \\ 0 & \text{otherwise} \end{cases} \quad (5)$$

Altogether, this leads to the final expression:

$$F(\theta, \phi_o) = \sum_{l=p+q}^{Mp+Nq} X_l \exp \left\{ j \frac{kd l \sin \theta}{\sqrt{p^2 + q^2}} \right\} \quad (6)$$

which is equivalent to the expression for the array factor of a linear array<sup>14</sup> where the excitation of each element is given by  $X_l$  with inter-element spacing

$$d_c = \frac{d}{\sqrt{p^2 + q^2}} \quad (7)$$

Essentially, this means that each  $\phi$ -cut of the planar array pattern is the same as the linear array pattern obtained by collapsing the excitations of the planar distribution on to the line  $\phi = \phi_o$ . Specifically, for the case of a square grid planar array, collapsing the antenna in any direction always yields an equispaced linear array. This is an essential property that is used in the present diagnosis method. For other geometries, like concentric circles, collapsing can result in non-equispaced linear arrays, and the method is not directly applicable.

### Detection of faulty elements

The method begins by directly applying the principle of collapsed distributions. The antenna is collapsed into the  $\phi = 0^\circ$ ,  $\phi = 90^\circ$  and  $\phi = 45^\circ$  axes. This yields three equispaced linear arrays with different number of elements and different inter-element spacing. For each array, all of the possible faulty patterns in which only one element is partially affected are tabulated. For each element in the linear array, 10 patterns are recorded in which the element excitation ranges from 0% until 90% of the original value  $I_n$ , in steps of 10%.

For an equispaced linear array laying in the xy plane, the far field pattern can be calculated by the following expression<sup>14,16</sup>:

$$F(\theta) = \sum_{n=1}^N I_n \exp \{j k d n \sin \theta\} = \sum_{n=1}^N H_n(\theta) \quad (8)$$

where  $I_n$  is the relative element excitation,  $k$  is the wavenumber,  $d$  is the inter-element spacing and  $H_n(\theta)$  is the directionally weighted phasor corresponding to the  $n$ th element of the array. Considering  $C$  to be the set containing the indexes of the faulty element, the degraded far field pattern  $F_C$  can then be calculated as follows:

$$F_C(\theta) = F(\theta) - \sum_{n \in C} 0.1 p_n H_n(\theta) \quad (9)$$

where  $p_n$  ranges from 0 (no failure) to 10 (complete failure). Assuming that the  $10 \times N$  patterns  $\{F_n^p(\theta)\}_{n=1, p=1}^{n=N, p=10}$  radiated by the array when only the  $n$ th element is failing by  $10 \times p\%$  are known, the pattern radiated by the defective array,  $F_C$ , can be calculated in terms of the error-free pattern and these partial single-faults patterns as

$$F_C(\theta) = F(\theta) - \sum_{n \in C} [F(\theta) - F_n^{p_n}(\theta)] \quad (10)$$

where

$$F_n^{p_n}(\theta) = F(\theta) - 0.1 p_n H_n(\theta), \quad n \in \{1, 2, \dots, 10\}, \quad p_n \in \{1, 2, \dots, 10\} \quad (11)$$

In order to begin the procedure of locating the defective elements, the degraded pattern of the antenna  $F_D(\theta)$  must be measured along each of the three  $\phi$  cuts mentioned above. For each cut,  $M$  equispaced samples are taken along the theta coordinate  $\{F_D(\theta_m)\}_{m=1}^M$ . With this information, the method compares the measured pattern with every possible pattern corresponding to the array with a given configuration of partially failing elements. This is done by performing an exhaustive search of the target configuration that minimizes the squared distance  $d_C$ :

$$d_C = \sum_{m=1}^M [F_D(\theta_m) - F_C(\theta_m)]^2 \quad (12)$$

The results of this search are three faulty linear arrays, which specify the indices of the failing elements along the x-axis, the y-axis and the  $\phi = 45^\circ$  axis, along with the percentage of failure of each index. With this information, and considering  $X$ ,  $Y$ ,  $X_{45}$  to be the sets containing the indices of the faulty elements along the three axes, the location of the defective elements of the planar array is reconstructed as follows:

1. Consider the set  $A$  containing all the possible combinations of taking one index from  $X$  and one from  $Y$ , so that the resulting projection on to the  $\phi = 45^\circ$  axis is compatible with  $X_{45}$ . These combinations are possible locations of the faulty elements in terms of XY coordinates.
2. Now consider the set  $comb(A)$  containing all combinations of the elements of  $A$  whose indices are compatible with  $X_{45}$ . These are the possible target configurations.
3. In order to discriminate from the configurations in  $comb(A)$ , the corresponding percentage failure of the indices along the x-axis and y-axis is calculated for each configuration. The configuration with the best match will be the final target.

Figure 2 presents a flow chart of the algorithm for better clarity.

As this may seem quite cumbersome, for a better understanding of the procedure, we can illustrate the method with an example, shown in Fig. 3, of the antenna used in the simulation. Our example configuration has failed elements in positions  $(x, y) = (7, 2), (8, 2), (8, 3)$ .

Applying the exhaustive search, which recovers the projection of the faulty elements on the three mentioned axes, the following indices and percentages of failure  $\Delta$  are obtained:

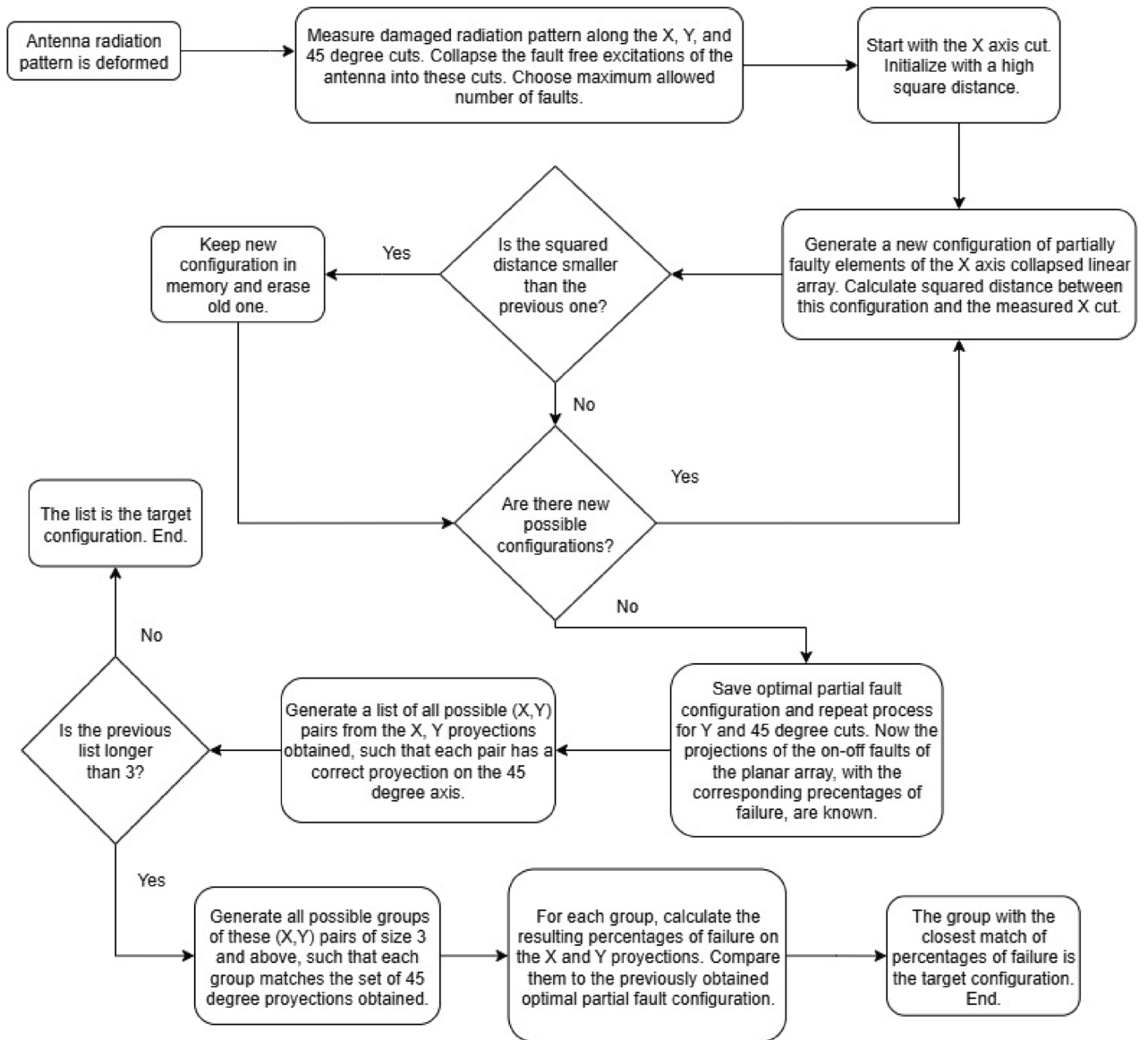


Fig. 2. Flow chart of the fault detection algorithm.

$$\begin{aligned}
 X &= \{7, 8\} & \Delta_X &= (0.9, 0.7) \\
 Y &= \{2, 3\} & \Delta_Y &= (0.6, 0.9) \\
 X_{45} &= \{5, 6, 7\} & \Delta_{X_{45}} &= (0.9, 0.9, 0.9)
 \end{aligned}
 \tag{13}$$

The corresponding set A is:

$$A = \{(7, 2), (7, 3), (8, 2), (8, 3)\}$$

The set comb(A) is then constructed:

$$comb(A) = \{[(7, 2), (7, 3), (8, 3)], [(7, 2), (8, 2), (8, 3)], [(7, 2), (7, 3), (8, 2), (8, 3)]\}$$

Of these three configurations, the one that best matches the percentages of failure is

$$[(7, 2), (8, 2), (8, 3)]$$

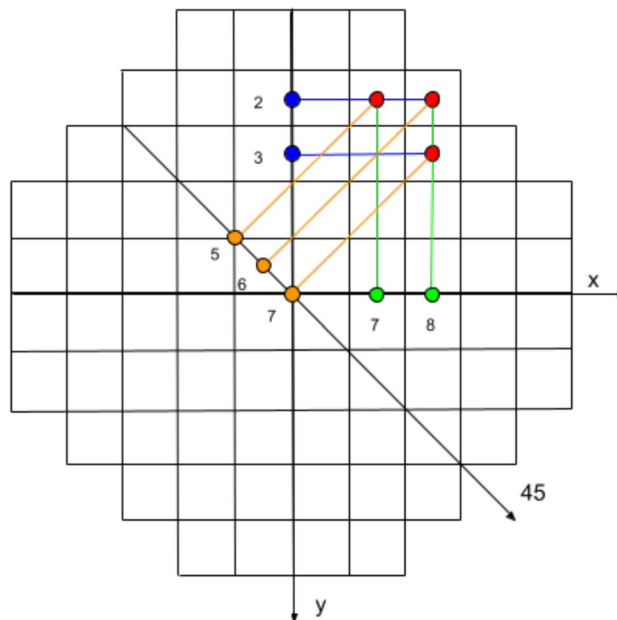


**Fig. 3.** Example of element failure in 76-element square grid antenna with circular boundary. Element excitations are shown in Fig. 1.

### Data availability

The datasets used and/or analysed during this study are available from the corresponding author upon reasonable request.

Received: 30 April 2025; Accepted: 3 November 2025

Published online: 03 December 2025

### References

- Hodges, R. E. & Rahmat-Samii, Y. On sampling continuous aperture distributions for discrete planar arrays. *IEEE Trans. Antennas Propag.* **44**, 1499–1508 (2002).
- Peters, T. A conjugate gradient-based algorithm to minimize the sidelobe level of planar arrays with element failures. *IEEE Trans. Antennas Propag.* **39**, 1497–1504 (1991).
- Rodríguez, J. A., Ares, F., Palacios, H. & Vassallo, J. Finding defective elements in planar arrays using genetic algorithms. *Prog. Electromagn. Res.* **29**, 25–37 (2000).
- Bucci, O., Capozzoli, A. & D’Elia, G. Diagnosis of array faults from far-field amplitude-only data. *IEEE Trans. Antennas Propag.* **48**, 647–652 (2000).
- Fuchs, B., Le Coq, L. & Migliore, M. D. Fast antenna array diagnosis from a small number of far-field measurements. *IEEE Trans. Antennas Propag.* **64**, 2227–2235 (2016).
- Salucci, M., Gelmini, A., Oliveri, G. & Massa, A. Planar array diagnosis by means of an advanced Bayesian compressive processing. *IEEE Trans. Antennas Propag.* **66**, 5892–5906 (2018).
- Palmeri, R. et al. Fault diagnosis of realistic arrays from a reduced number of phaseless near-field measurements. *IEEE Trans. Antennas Propag.* **71**, 7206–7219 (2023).
- Bréguins, J., Ares, F. & Moreno, E. Matrix pseudo-inversion technique for diagnostics of planar arrays. *Electron. Lett.* **41**, 7–8 (2005).
- Iglesias, R. et al. Element failure detection in linear antenna arrays using case-based reasoning. *IEEE Antennas Propag. Mag.* **50**, 198–204 (2008).
- Morabito, A., Palmeri, R. & Isernia, T. A compressive-sensing-inspired procedure for array antenna diagnostics by a small number of phaseless measurements. *IEEE Trans. Antennas Propag.* **64**, 3260–3265 (2016).
- Palmeri, R., Isernia, T. & Morabito, A. F. Diagnosis of planar arrays through phaseless measurements and sparsity promotion. *IEEE Antennas Wirel. Propag. Lett.* **18**, 1273–1277 (2019).
- Wang, Z. A. & Li, P. Phaseless diagnosis and pattern correction of faulty antenna arrays via advanced Bayesian compressive sensing approaches. *Electromagn. Sci.* **3**, 0090382–1 (2025).
- Kim, Y. U. *Antenna Array Patterns: Analysis and Synthesis*, PhD dissertation (University of California, Los Angeles, 1987).
- Elliott, R. S. *Antenna Theory and Design* (Wiley, 2006).
- Illade-Quinteiro, J., Rodríguez-González, J. & Ares-Pena, F. Shaped-pattern synthesis by spreading out collapsed distributions. *IEEE Ant Propag M.* **52**, 110–114 (2010).
- Rodríguez-González, J. A., Ares-Pena, F., Fernández-Delgado, M., Iglesias, R. & Barro, S. Rapid method for finding faulty elements in antenna arrays using far field pattern samples. *IEEE Trans. Antennas Propag.* **57**, 1679–1683 (2009).

### Acknowledgements

This work was partly supported by the FEDER / Ministerio de Ciencia e Innovación - Agencia Estatal de Investigación under Project PID2020-119788RB-100/AEI/10.13039/501100011033. The authors thank professors Tommaso Isernia, Marco Donald Migliore and Andrea Massa for sharing their articles related to the topics addressed in this paper.

### Author contributions

Conceptualization, F.J.A.-P.; methodology, D.M.P.-O., J.A.R.-G., M.E.L.-M., and F.J.A.-P.; validation, D.M.P.-O. and F.J.A.-P.; investigation, D.M.P.-O.; resources, F.J.A.-P. and J.A.R.-G.; writing-original draft presentation, D.M.P.-O.; writing-review and editing; D.M.P.-O., J.A.R.-G., M.E.L.-M. and F.J.A.-P.; visualization, D.M.P.-O.; supervision, J.A.R.-G., M.E.L.-M., and F.J.A.-P.; project administration, F.J.A.-P. and M.E.L.-M.; funding acquisition, F.J.A.-P. and M.E.L.-M. All authors have read and agreed to the published version of the manuscript. Correspondence and requests for material should be addressed to F.J.A.-P.

### Declarations

### Competing interests

The authors declare no competing interests.

### Additional information

**Correspondence** and requests for materials should be addressed to F.J.A.-P.

**Reprints and permissions information** is available at [www.nature.com/reprints](http://www.nature.com/reprints).

**Publisher's note** Springer Nature remains neutral with regard to jurisdictional claims in published maps and institutional affiliations.

**Open Access** This article is licensed under a Creative Commons Attribution-NonCommercial-NoDerivatives 4.0 International License, which permits any non-commercial use, sharing, distribution and reproduction in any medium or format, as long as you give appropriate credit to the original author(s) and the source, provide a link to the Creative Commons licence, and indicate if you modified the licensed material. You do not have permission under this licence to share adapted material derived from this article or parts of it. The images or other third party material in this article are included in the article's Creative Commons licence, unless indicated otherwise in a credit line to the material. If material is not included in the article's Creative Commons licence and your intended use is not permitted by statutory regulation or exceeds the permitted use, you will need to obtain permission directly from the copyright holder. To view a copy of this licence, visit <http://creativecommons.org/licenses/by-nc-nd/4.0/>.

© The Author(s) 2025